Proceedings of the ASME 2010 International Manufacturing Science and Engineering Conference
MSEC2010
October 12-15, 2010, Erie, Pennsylvania, USA

MSEC2010-' (&+)

THE EFFECTS OF EMISSIVITY AND CAMERA POINT SPREAD FUNCTION ON THE TEMPERATURE MEASUREMENT OF SEGMENTED CHIP FORMATION USING INFRARED THERMOGRAPHY

Jarred C. Heigel
KT Consulting, Inc.
Lexington, KY, USA
jarred.heigel@gmail.com

Eric P. Whitenton
National Institute of Standards and Technology[1]
Gaithersburg, MD, USA
eric.whitenton@nist.gov

ABSTRACT

This paper uses simulation to investigate measurement errors resulting from the camera point spread function (PSF) when measuring the temperature of segmented chip formation using infrared (IR) thermography. The PSF of the IR camera effectively filters the results which can cause significant errors due to the large temperature gradients and abrupt transitions between features and their corresponding emissivity values. The different emissivity values of the tool, workpiece, chip body, and shear band affect the apparent difference in the emitted energy of these different features. This decreases the measured temperature in the regions of most interest: along the tool-chip interface and the periodic shear zone. The method in this study creates an appropriate emissivity map from post-process measurements and applies it to results from the temperature distribution of the cutting zone predicted by commercial finite element analysis (FEA) software. Comparisons between the simulation results and experiment results show that the emissivity values obtained form the post process chip analysis lead to good agreement. The resulting radiant intensity distribution becomes the input for an IR camera simulation module developed by the authors and presented in earlier work [1]. The earlier work used the true temperature distribution predicted by the FEA as the simulation module input, and did not incorporate the IR camera's PSF. Implementation of the actual IR camera's PSF allows the simulation module to more accurately represent the measurements of the IR camera and ultimately allow the comparison of the simulation results to the measurement results. Simulation results show that the PSF accounts for 45 % of the 42 °C radiance temperature error at the tool-chip contact along the rake face. The PSF accounts for approximately 15 % of the 46 °C radiance temperature measurement error at a point in the center of the catastrophic shear band. These errors consider the effects of motion blur (integration time) and magnification (size-of-source), as described in the earlier work [1].

INTRODUCTION

Understanding the temperatures resulting from the metal cutting process leads to improvements in process efficiency. First, cutting temperature affects the dimensional accuracy and surface properties of the part and "adversely affects the strength, hardness, and wear resistance of the cutting tool" [2]. Tool coating and substrate materials, as well as cutting parameters such as rake, speed, and feed, can be optimized to reduce the temperatures and increase tool life. Second, models of the cutting process rely on temperature dependent material properties [3, 4]. Flow stress has been shown to decrease with increasing temperature. By understanding the temperatures experienced in metal cutting, material property tests can be performed at the appropriate temperatures and heating rates [5, 6]. Additionally, accurate measurements of metal cutting

[1] This paper is an official contribution of the National Institute of Standards and Technology and is not subject to copyright in the United States. Commercial equipment and materials are identified in order to adequately specify certain procedures. In no case does such identification imply recommendation or endorsement by the National Institute of Standards and Technology, nor does it imply that the materials or equipment are necessarily the best available for the purpose.

Copyright © 2010 by ASME
This work is in part a work of the U.S. Government. ASME disclaims all interest in the U.S. Government's contributions.

temperatures and forces provide benchmarks against which researchers in the modeling community can calibrate their models. Metal cutting models assist in the design of new tooling and the optimization of cutting processes.

Measurement error and uncertainty must be understood to properly interpret infrared (IR) thermography measurements of the metal cutting process [7, 8]. The dynamic character of segmented chip formation complicates temperature measurement [9, 10]. Specifically, the periodic shear band exhibits high thermal gradients in space and time, small feature sizes, and high accelerations and velocities. Consequently, the temperatures measured for these bands depend on the emissive properties of the bands and the surrounding chip, the time duration and the observation area of the measurement, and the point-spread function (PSF) of the camera. In addition to complications in measuring the shear band, the different emissivity values of the tool and the chip, combined with the effects of the PSF, make determining the temperature along the rake face difficult.

An earlier study by the authors investigated the errors associated with the integration time and size-of-source of a simulated ideal IR camera measuring a simulated cutting zone with an emissivity value of 1 [1]. Size-of-source refers to the area measured by a single camera sensor; it is directly related to the magnification. The study investigated a range of integration times and pixel element areas and found that integration time significantly affected the measurement results in the shear band as the ratio of integration time to segment period increases; however, the rake measurements were relatively unaffected.

The current study improves upon the earlier methodology to include the emissivity values of the different features in the cutting zone. Post-process analysis of the chip and cutting tool provides these emissivity values. An emissivity map is created and applied to a known dynamic temperature field, created by a commercial finite element analysis (FEA) software package. The resulting intensity distribution is then sampled by the simulated IR camera. This is a necessary step because of the non-linear relationship between temperature and intensity. Although the FEA may not produce the exact conditions experienced in the metal cutting experiments imaged by the IR camera, the FEA results have been shown to adequately represent the periodicity of segmented chip formation with temperature gradients similar to those expected in the actual process [11]. The study also includes the PSF of the camera used in the ongoing dual-spectrum high-speed microvideography research at the National Institute of Standards and Technology (NIST) [8-15]. This process makes the simulation specific to the NIST setup and allows comparison of the simulation results and experimental results.

DUAL-SPECTRUM MEASUREMENT

This section presents an overview of the dual-spectrum high-speed microvideography camera system at NIST. In addition, it presents the PSF of the IR camera and determination of the tool emissivity and chip emissivity. Measurement results are presented later when compared to the simulation results.

Cutting Conditions

Workpieces are 3 mm thick, 127 mm diameter discs cut from American Iron and Steel Institute (AISI) 1045 cold-drawn steel rods. Grinding the disc surfaces ensures parallelism necessary to maintain focus. A Seco-Carboloy TNMG220408-MR4 CP25 triangular insert, held in a -7° rake angle MTCNN443 tool holder and attached to the face of a 3-axis dynamometer, provides the orthogonal cutting edge for the experiments. The corner of the insert imaged by the camera system is ground to provide a flat surface for imaging, removing the coating and revealing the tungsten carbide. The chip forms as close to the ground edge as possible without affecting the chip formation. The cutting test used for comparison was performed with a surface speed of 250 m/min and a feed of 0.3 mm.

Camera Setup

Current work at NIST uses a dual-spectrum high-speed camera system to observe and measure the cutting process. A brief overview of the camera system will be presented. Detailed information on the camera system and the accompanying work can be found in references [8-15]. Figure 1 shows the experimental setup.

The camera system images the side of an orthogonal cutting process. The infrared camera in the dual-spectrum system obtains radiant intensity at 600 frames per second (fps). The camera bandwidth dictates that at the chosen frame rate the camera uses a portion of the focal plane array (FPA) 160 sensors wide and 120 sensors tall. The field of view is 0.96 mm wide and 0.72 mm tall. Assuming 100 % coverage, each sensor element in the FPA observes an area of 35 μm^2 (in reality FPAs have less than 100 % coverage, resulting in a smaller area imaged by each sensor). A wavelength limiting filter is not used. By observing a large range of wavelengths (3.8 μm to 5.1 μm in

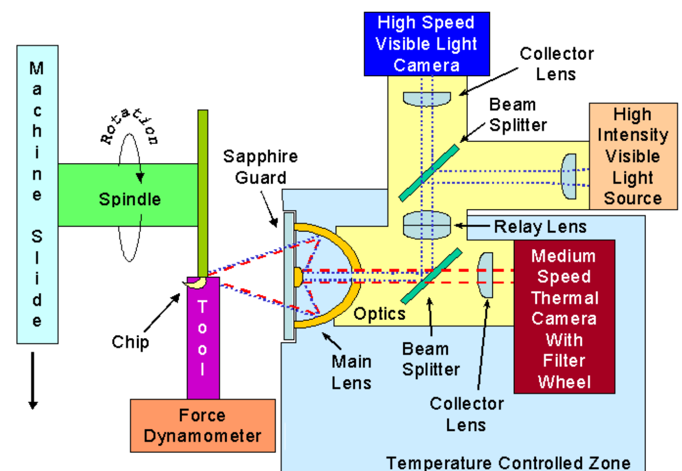

FIGURE 1. HIGH-SPEED DUAL-SPECTRUM SETUP.

Copyright © 2010 by ASME

this case), fast integration times can be used to minimize "motion blur." Planck's equation (Equation 1) converts the infrared intensity (I in W/sr·μm^2) of the range of wavelengths (λ_1 and λ_2 in μm) into radiant temperature (T in K).

$$I = \int_{\lambda_1}^{\lambda_2} \frac{c_{1L}/\lambda^5}{e^{\frac{c_2}{\lambda T}} - 1} d\lambda \quad (1)$$

c_{1L} describes the first radiation constant and has a value of $1.191 \cdot 10^{-4}$ W·μm^2. The constant c_2 has the value of 14387.752 μm·K.

A high-speed visible camera, set at a frame rate of 30 000 frames per second (fps), uses the same main optic to observe the chip formation process. This allows mapping the thermal field obtained by the IR camera to the physical features of the chip formation process recorded by the visible light camera.

IR Camera Point Spread Function

A PSF is a curve characterizing the response of the imaging system to a point source. The measurement of the narrow shear band as well as other features with large gradients in temperature or emissivity can be significantly affected by the PSF. Therefore, a proper simulation of the camera system requires inclusion of the PSF. The IR camera's PSF has been determined using the knife-edge method [15]. This method incorporates the effects of the optical elements in series with the IR camera in the system. A graphical representation of the PSF is presented in Figure 2.

Determining Emissivity

Emissivity estimation remains a challenge when making temperature measurements in the infrared light spectrum. Published emissivity values obtained under ideal conditions are inadequate. The surface's varying structure and roughness combined with oxidation effects necessitate characterizing the emissivity within the desired region of interest. Additionally, the emissivity can change with temperature.

Chip Emissivity The emissivity values used in this study are measured from steel chips obtained from two different cutting tests. These chips represent the upper and lower bounds

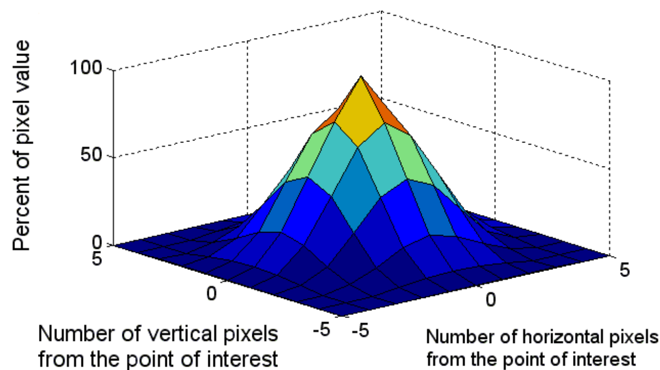

FIGURE 2. IR CAMERA PSF REPRESENTATION.

of the emissivity values observed in the post process chips. The difference in emissivity between the two chips is most likely caused by oxidation. A significant part of the oxidation probably occurred after the chip left the camera's field of view during cutting. However, because the oxidation process during metal cutting and its effects on the chip emissivity at the instance imaged by the IR camera are unknown, both emissivity value sets are used in the analysis. Figure 3 presents visible and IR images of the chips used in this analysis.

To measure the emissivity, a chip and a thermocouple are placed in a pin vice so that the side of the chip, corresponding to the same surface exposed to the camera during testing, can be imaged with the dual-spectrum camera system. The pin vice is then resistively heated to achieve a chip temperature approximating the temperature experienced during cutting. This temperature is verified with the thermocouple. Assuming temperature equilibrium within the chip and thermocouple, the true temperature is known. While at constant temperature, the dual-spectrum camera system images the side of the chip. Knowing the radiance temperature measured by each pixel of the infrared camera and the temperature recorded by the thermocouple allows determination of the emissivity at each pixel of the infrared image using Equation 2.

$$I_{apparent} = \varepsilon \cdot I_{true} + (1-\varepsilon) \cdot I_{environment} \quad (2)$$

ε represents the emissivity value. $I_{apparent}$ uses Equation 1 where T is the temperature of a single IR image pixel. I_{true} uses Equation 1 where T is the measured temperature of the thermocouple. $I_{environment}$ uses Equation 1 where T is the temperature of the surroundings. $I_{environment}$ accounts for reflections from the surrounding environment, and thus uses 293 K as the temperature of the laboratory.

Emissivity of the desired regions (the fissures between segments, and the body of the segments) is characterized by

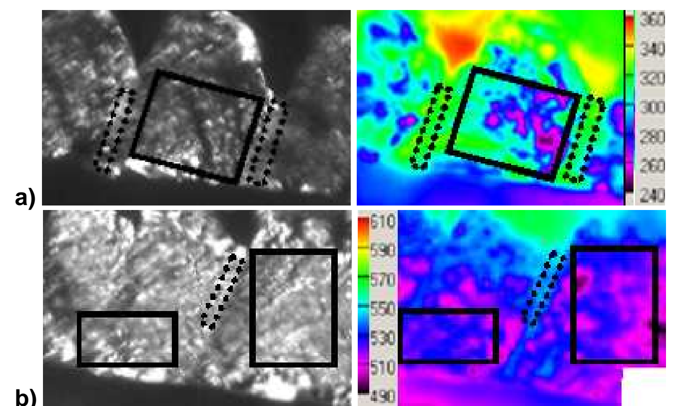

FIGURE 3. VISIBLE AND IR IMAGES OF THE CHIPS USED TO DETERMINE EMISSIVITY. SOLID BOXES MARK CHIP BODY REGIONS, DOTTED BOXES MARK SHEAR BAND REGIONS. THERMOCOUPLE MEASUREMENTS FOR a) CHIP 1 IS 391 °C AND b) CHIP 2 IS 570°C. TEMPERATURE SCALES IN RADIANCE °C.

Copyright © 2010 by ASME

calculating the average and standard deviation of the emissivity values within the appropriate regions of interest in the emissivity map, indicated by rectangles in Figure 3.

Table 1 presents the results of this analysis. Chip 1 is assumed to have a thinner oxide layer than chip 2 due to the lower emissivity values. Therefore, the assumption is made that chip 1 better represents the chip condition immediately after formation in the cutting zone, since the oxidation process is time dependent and would not have developed a significantly thick layer to affect the chip emissivity.

Tool Emissivity A similar method is used to determine the tool emissivity. Characterization of the tool proves to be simpler because the characteristics of the side of the tool do not significantly change during the test. Experience from prior experimentation has shown that an oxide layer tends to develop on the side of the exposed tungsten carbide substrate (on the ground surface) as a result of the cutting process. Therefore, a pre-oxidized tool is used for both machining experiments and emissivity determination. Figure 4 presents an IR image of the side of a Kennametal[1] A4G0605M06U04B grooving tool, with a mean emissivity of 0.58 and a standard deviation of 0.06. The large apparent temperature gradient, despite an assumed constant true temperature of 292 °C throughout the tool, is due to an uneven oxide buildup developed during the cutting tests. For this study, it is assumed that the emissivity of the oxidized tungsten carbide is the same for this insert and the insert used for the cutting test.

SIMULATION OF THE INFRARED CAMERA

This section describes the necessary steps to simulate the IR camera. It begins by using the commercial FEA software to generate a sequence of temperature images of the cutting process with high spatial and temporal resolution. The temperature field data is then converted into radiant energy fields using the emissivity characteristics of the chip features and the insert. Finally, the radiant energy is "measured" by the simulated IR camera, which incorporates the effects of the PSF.

TABLE 1. POST-PROCESS CHIP EMISSIVITY VALUES.

Chip	Region	Emissivity value	
		mean	standard deviation
1	chip body	0.42	0.07
1	fissure	0.53	0.05
2	chip body	0.77	0.03
2	fissure	0.85	0.02

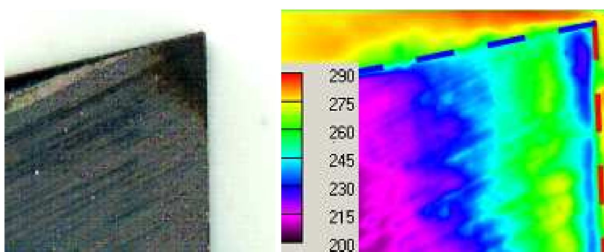

FIGURE 4. VISIBLE AND IR IMAGES OF THE INSERT USED TO DETERMINE THE TOOL EMISSIVITY MAP. THE RED DASHED LINE REPRESENTS THE RAKE EDGE, THE BLUE DASHED LINE REPRESENTS THE CLEARANCE EDGE. TEMPERATURE SCALE IN RADIANCE °C.

Finite Element Analysis Simulation

The known dynamic temperature field for the IR camera simulation comes from a two-dimensional turning simulation obtained with Third Wave Systems' Advantedge software[1]. Prior work has shown that the simulation of AISI 1045 steel produces segmented chips with comparable segmentation periods to the experimental data [11].

The simulation parameters can be found in Table 2. These parameters were chosen so that the time between each frame output by the simulation corresponds to 0.2 µs. One segment forms in about 90 µs. This high sampling rate provides a fine temporal thermal field evolution of a single segment. Only one segment is needed because the simulation results do not exhibit significant randomness in the segmentation process. The individual node values of the FEA simulation are not evenly spaced and change due to velocity and dynamic re-meshing. Therefore, the thermal field results are exported as an audio video interleave (AVI) movie to provide a grid of equally spaced data points to be used for the IR camera simulation.

FEA Temperature Conversion to Radiated Intensity

Temperature data from the FEA analysis is converted into radiant energy by applying the chip emissivity information in Table 1, using Equation 3, according to the features in each AVI frame.

$$I = \varepsilon \cdot \int_{\lambda_1}^{\lambda_2} \frac{c_{1L} / \lambda^5}{e^{\frac{c_2}{\lambda T}} - 1} d\lambda \qquad (3)$$

TABLE 2. FEA SIMULATION PARAMETERS.

Workpiece	
Material:	AISI-1045 (200 Bhn)
Workpiece height (mm):	2
Workpiece length (mm):	10

Process parameters	
Feed (mm)	0.3
Depth of cut (mm)	1
Length of cut (mm)	3
Cutting speed (m/min)	250
Initial temperature (°C)	20

Simulation parameters: General	
Simulation mode:	Standard

Tool	
Material:	Carbide - General
Rake angle (°):	-7
Clearance angle (°):	7
Edge radius (µm):	20
Maximum tool element size (mm):	0.3
Minimum tool element size (mm):	0.03
Mesh grading:	0.4

Simulation parameters: Results	
Number of output frames	15
Number of windows	1
Window start (mm)	1.579
Window finish (mm)	1.958

Simulation parameters: Workpiece meshing	
Maximum number of nodes:	150000
Suggested maximum element size (mm):	0.2
Suggested minimum element size (mm):	0.01
Cutting edge radius to determine minimum element size (mm):	0.8
Feed fraction to determine minimum element size:	0.1
Mesh refinement factor:	8 (fine)
Mesh coarsening factor:	4

Copyright © 2010 by ASME

This is necessary because in reality, an object does not emit all the radiant energy theoretically possible due to temperature. Instead, it emits radiant energy based on the temperature and an efficiency factor, which ranges between 0 and 1, called the emissivity. Simulation of the radiant energy is necessary due to the non-linear relationship between T and I. The tool emissivity characteristics displayed in Figure 4 can simply be applied to the tool in the FEA results, since the tool does not move or change in the simulation. However, applying emissivity to the chip features and the workpiece is more complicated because they are developing and moving. Figure 5a through Figure 5c present sample images of the FEA generated temperature field, strain field, and strain-rate field. This information is used to classify portions of the thermal images as either workpiece, chip body, shear band, or undefined. The undefined portions are assigned an emissivity value of zero. The workpiece, chip body, and shear band portions are assigned emissivity values by an empirically derived procedure described next.

Create Emissivity Maps for Each Feature The process begins by creating a small emissivity map for each feature (workpiece, chip body, and shear band) using the values in Table 1 as samples from a normal distribution. The workpiece emissivity has not been characterized and thus arbitrary values are used for the mean and standard deviation (0.40 and 0.03, respectively). Ultimately, the workpiece emissivity values have little impact since the actual IR camera cannot measure the workpiece temperature due to the camera settings chosen. After creating the small emissivity maps, they are enlarged by a certain amount using the MATLAB "imresize" function. This makes the image look less like white noise and more like the surface of the chip. This can be seen when observing the features in Figure 5d.

Assigning the Chip and Workpiece Emissivity Values The plastic strain data dictates how to combine the workpiece and chip body emissivity maps. The amount of plastic strain indicates whether the chip emissivity or workpiece emissivity is applicable. Data points with a plastic strain $\geq$ 0.5 use 100 % of the chip emissivity map, while data points with plastic strain $\leq$ 0.3 use 100 % of the workpiece emissivity map. Data points with plastic strain between these values use a linear relationship to determine the percentages of the chip and workpiece emissivity maps to use.

Assigning the Shear Band Emissivity Values The plastic strain rate is used to identify the shear band. Strain rate is used instead of strain because the dynamic re-meshing used in the FEA distorts the strain data of the shear band after it is formed. This can be seen in the lower edge of Figure 5b. Because this study only assesses the shear band during its development, the fully developed shear band is ignored. Plastic strain rate $\geq 30\,000\ s^{-1}$ dictates 100% of the shear band emissivity, while plastic strain rate $\leq 6\,000\ s^{-1}$ dictates 100% of the chip body emissivity. Once again, data points with plastic strain rate between these values use a linear relationship to determine the percentages of the chip and shear band emissivity maps to use.

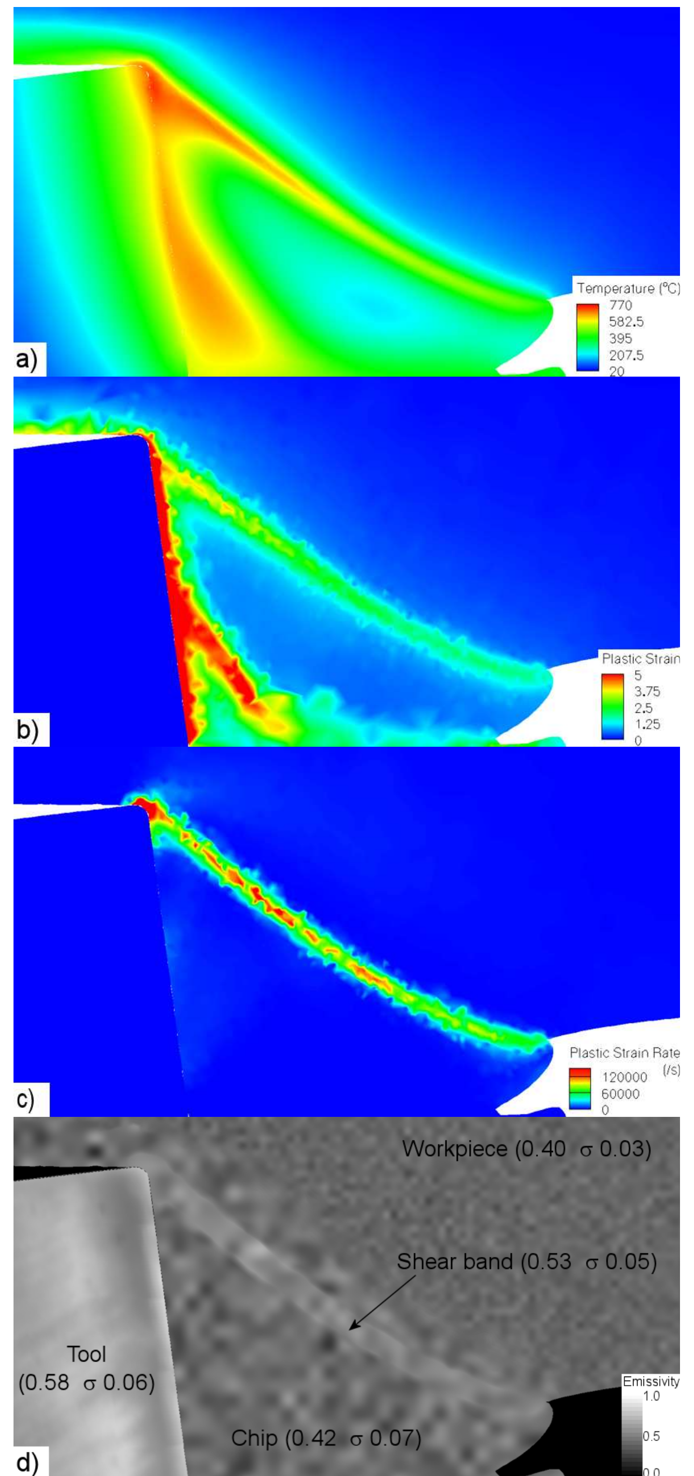

FIGURE 5. a) TEMPERATURE FIELD, b) PLASTIC STRAIN FIELD, AND c) PLASTIC STRAIN-RATE FIELD FROM A SINGLE TIME INSTANCE OF THE FEA RESULTS. d) THE RESULTING EMISSIVITY MAP WITH MEAN EMISSIVITY AND STANDARD DEVIATION (σ).

Copyright © 2010 by ASME

Shifting the Emissivity Maps with the Movement To account for the velocity of the chip and the workpiece, the individual emissivity maps need to be shifted consistent with the feature velocities. The workpiece emissivity map is shifted according to the average horizontal velocity component in a region of workpiece data not affected by the chip formation process. Similarly, the chip body emissivity map is shifted by the average of the horizontal and vertical velocity components of the chip after formation. The shear band emissivity map is shifted by the two velocity components in the shear band determined by the shear rate criteria.

IR Camera Simulation

This section discusses the method used for simulating an infrared camera measurement. A detailed explanation of an earlier version of the IR camera simulation can be found in the previous work [1]. The camera simulation considers integration time, size-of-source (relative pixel to feature size), and now considers the camera PSF and uses radiance intensity instead of temperature as an input, as described earlier. The earlier work considered a range of integration times and size-of-source relationships to show how changing these values affect the measurement error. In this study, an integration time of 10 µs is used to mimic the experimental conditions used for comparison. This means that 50 FEA simulation frames are used to simulate one IR camera frame. Furthermore, the magnification used in the experiment causes each IR camera sensor to observe a 35 μm^2 area of the target. Therefore, the same size is used in the simulation, equating to a simulated IR sensor integrating a 9 pixel by 9 pixel area in the radiant intensity frame. After this, the PSF is applied to the array of simulated IR sensors. Figure 6 presents a schematic of the IR camera simulation process.

RESULTS

Simulation results are first compared to experimental results to illustrate how well the FEA and the IR camera simulation approximate the IR measurement of the actual cutting process. Next, the measurement errors estimated by the IR camera simulation are presented. In addition, the impact of including the PSF in the simulation is assessed to understand the importance of properly characterizing the IR camera.

- Account for integration time using a loop to create 50 90 x 100 images.

  for i=1:50 (required FEA simulation frames for 10 µs)
    - Load radiant intensity image # i.
    - Break the radiant intensity image into 9 x 9 pixel groups. Integrate each pixel group to calculate the value emitted to the corresponding simulated IR sensor, creating a new array. This accounts for size-of-source and creates the 90 x 100 image.
    - Apply the PSF to the newly developed image.

  end
- Calculate the average intensity value of all images for each pixel to create the radiant temperature field measured by the simulated IR camera. This accounts for motion blur.
- Convert the radiant intensity field into radiant temperature using Equation 1.

FIGURE 6. SIMPLIFIED IR CAMERA SIMULATION.

Comparison of Simulation and Experimental Results

When performing thermal measurements of the chip formation process, two features are typically of interest: the temperature of the chip along the tool rake face and the temperature of the shear band.

Chip Temperature Near the Tool Rake Face Friction between the tool and chip and high local shear contributes to heat generation in the chip. Measurement and simulation of the temperature generation, indicative of the "friction" behavior, are essential for intelligent tool design and process parameter selection. Figure 7 presents three plots comparing the temperature distribution of the chip at various distances from the rake face from the experimental results and simulation results using emissivity values from chip 1 and chip 2 in Table 2.

The plots in Figure 7 are formed by applying an analysis grid to the chip projecting from the insert rake face in the IR camera images (both real and simulated) [13]. This approach allows the temperature values in each grid square to be averaged together, smoothing the data and minimizing noise effects. Grid section dimensions of 3 pixels x 3 pixels maintain adequate analysis resolution. The camera's minimum measurable radiant temperature (300 °C, a result of integration rate) would artificially inflate the average chip temperature values in certain areas because temperatures below the minimum value are ignored. To eliminate this effect, all values in a given grid area must be greater than the 300 °C minimum for the grid area to be considered usable. This was not a concern for the simulation profiles. The temperature profile closest to the tool rake face in the experimental results (blue curve labeled 7.5 µm in Figure 7a) exhibits vertical bars which represent the standard deviation of the measured radiance temperature values of a single cutting test used to create this curve. Bars were not included on the corresponding curves for the simulation results because the maximum standard deviation is less than 10 °C, which does not register on the chosen plot scale.

Comparison of the plots in Figure 7 reveals which chip emissivity values lead to better simulation results. The larger emissivity values of chip 2 lead to radiant temperature profiles closer to the measured profiles. However, the temperature profile closest to the rake surface remains about 100 °C less than the measured peak temperature. Other discrepancies are apparent when comparing Figure 7a and Figure 7c. The temperatures of each profile are greater in the experiment results than in the simulation results. Also, there is a greater variation between temperature profiles in the experimental results (Figure 7a) than in the simulations (Figure 7c).

Copyright © 2010 by ASME

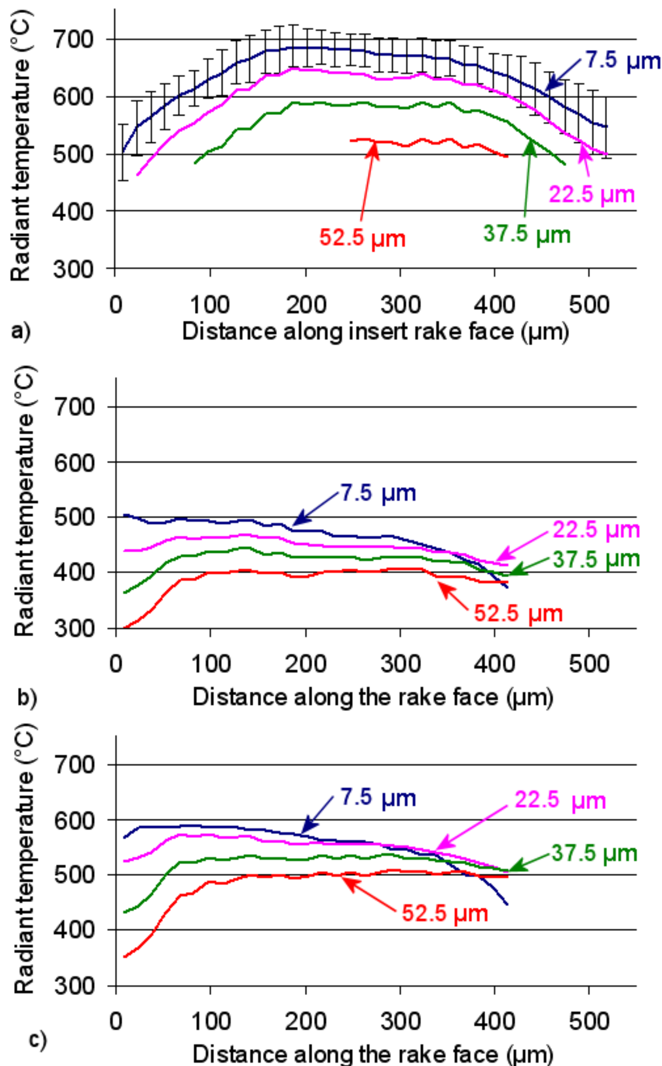

FIGURE 7. CHIP TEMPERATURE PROFILE AT VARYING DEPTHS INTO THE CHIP AS MEASURED FROM THE RAKE SURFACE. a) EXPERIMENTALLY MEASURED DATA, ERROR BARS ARE EXPLAINED IN THE TEXT.
b) SIMULATED DATA USING CHIP 1 EMISSIVITY VALUES.
c) SIMULATED DATA USING CHIP 2 EMISSIVITY VALUES.

Catastrophic Shear Band Temperature Comparing shear band temperature is difficult because of the difficulty involved in determining the evolution of the observed shear band in the dual-spectrum images. Although the accompanying high-speed visible image helps to verify that the feature observed in the IR image is in-fact a shear band, it does not have the resolution to determine how far the shear band has developed. Figure 8 presents some visible and IR images obtained using the dual-spectrum system. The shear band in Figure 8c-d is assumed to be fully developed such that shear has ceased and therefore so has heat generation. The shear band in Figure 8e-f has been formed and moved by the formation of the next segment. The shear band in Figure 8a-b is considered to be in the process of developing. The following analysis uses images from the experimentally obtained IR measurement that show a shear band that is in the process of developing or fully developed but not moved, determined by the location of the shear band in the images compared to the reference fully developed shear band in Figure 8c-d.

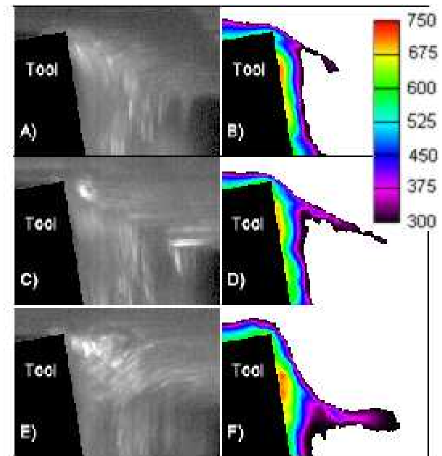

FIGURE 8. EXAMPLE DUAL-SPECTRUM IMAGES. THE BLACKED-OUT TOOL PROVIDES A VISUAL REFERENCE. TEMPERATURE SCALE IN RADIANCE ℃.

Figure 9 presents a comparison of shear band temperature for the experiment measurement, and simulations using emissivity values from chip 1 and chip 2 in Table 2. Figure 9a shows the temperature obtained from a curve drawn through the center of several shear bands that met the above requirements. Figure 9b-c shows the temperature at the center of a single shear band at several different instances in its development.

In contrast to the chip temperature analysis near the rake face, the emissivity values of chip 1 (Table 1) lead to better agreements in shear band radiant temperature between the measured values and simulated values. Interestingly, the shear band emissivity standard deviation appears to be greater in the experiment measurement than in the chips used to determine the emissivity values, judging by the variation in the curves in Figure 9. This may be a function of only using one post-process chip (in each case) with one or two shear band fissures to represent the much larger sample size of shear band fissures created during a cutting test. As expected when considering the results of the previous analysis, the radiant temperature in the shear band near the tool tip is larger for the measured values than for the simulated values. However, for temperatures at distances greater than 20 pixels (100 μm) from the tool tip, there is good agreement between the experiment and simulation results. It should be noted that the chips created in the cutting experiment are thicker than those in the FEA simulation. This could explain the longer curves in Figure 9a compared to Figure 9b-c. It would require significant changes to the material property parameters and/or model in the FEA software to obtain chips that more closely match the thickness of the chips

Copyright © 2010 by ASME

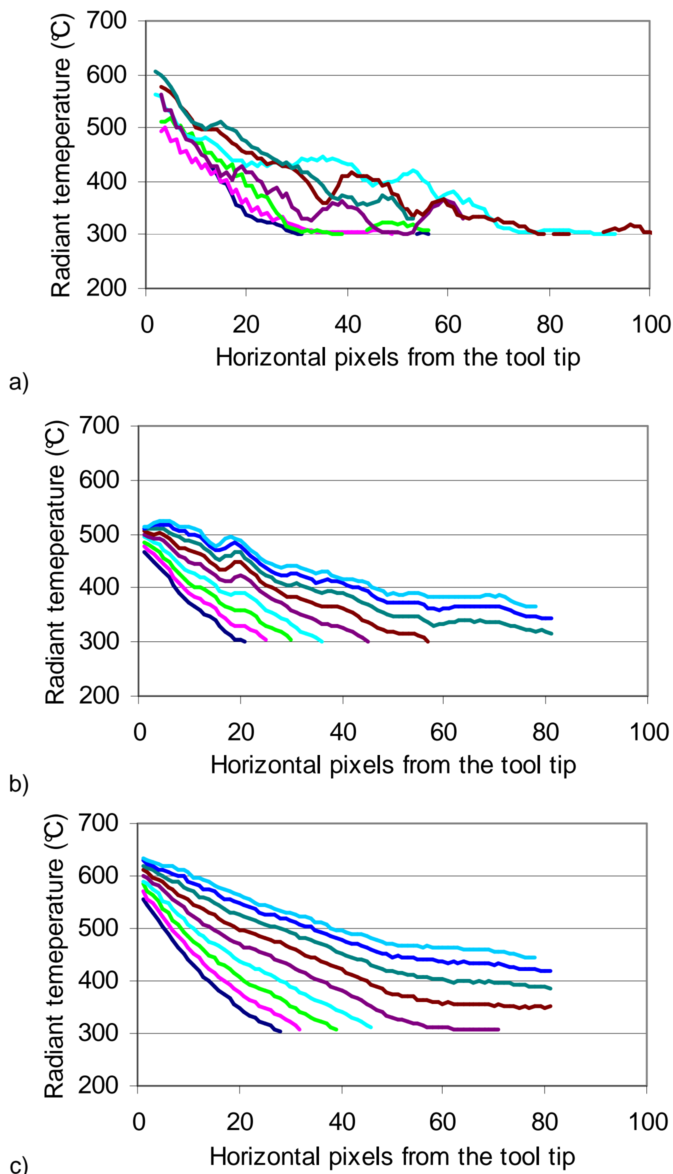

FIGURE 9. COMPARISON OF THE TEMPERATURE IN THE SHEAR BAND FOR a) EXPERIMENTALLY MEASURED DATA. b) SIMULATED DATA USING CHIP 1 EMISSIVITY VALUES. c) SIMULATED DATA USING CHIP 2 EMISSIVITY VALUES.

observed in the experiments while maintaining similar segmentation behavior. Because an exact match between the simulated and experimental chips is not required for the scope of this paper, the FEA material properties were not adjusted to create chips that more closely represented those developed in the cutting experiments.

Simulation Measurement Error

This analysis assumes that the maximum temperatures are the desired values from the FEA images. Thus, the measurement error is determined by subtracting the maximum radiant temperature from the FEA simulation within the 9 x 9 grid for all images within the integration time from the corresponding simulated IR camera pixel radiant temperature value. Measurement error is calculated for both chip emissivity sets under two IR camera simulation cases: 1) implementing the camera PSF in addition to integration time, size-of-source, and variable emissivity; 2) neglecting the camera PSF but still considering integration time, size-of-source, and variable emissivity. This provides insight into the significance of measurement error attributable to the camera optical effects described by the PSF.

Figure 10 presents measurement error images with the shear band fully developed (top curves in Figure 9b-c). Figure 10a and Figure 10b show the results of case 1, as described above. Figure 10c and Figure 10d illustrate the portion of the measurement error attributable to the PSF by subtracting the results of case 2 from the results of case 1. The analysis lines shown in Figure 10 illustrate where data is extracted to make the plots in Figure 11 in an effort to better illustrate the measurement error near the rake face and shear band. In an effort to simplify the analysis, analysis of the measurement error of the rake face and shear band is performed only on the simulation using the chip emissivity values determined to be a better fit according to the earlier analysis.

Figure 10a and Figure 10b show that the different chip emissivity values used in this study do not significantly affect the overall measurement error of radiance temperature. Observing the darker color along the rake edge in Figure 10a compared to Figure 10b, it is apparent that a greater measurement error exists along the rake face for the simulation using the chip 1 emissivity values, which are lower than the chip 2 values. This results from the greater difference between the tool emissivity and the chip body emissivity. Interestingly,

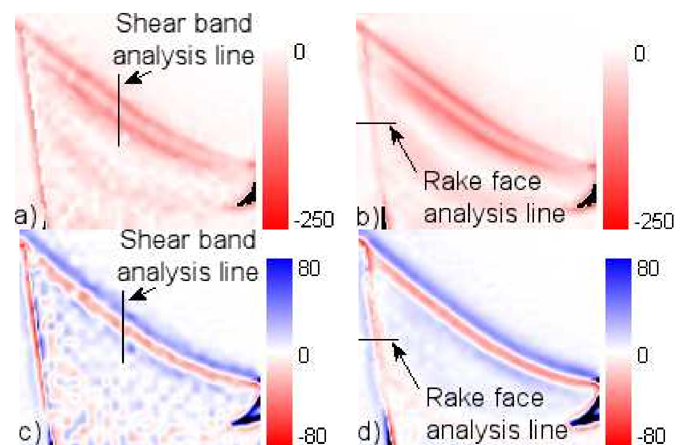

FIGURE 10. SIMULATION MEASUREMENT ERROR USING a) CHIP 1 EMISSIVITY VALUES AND b) CHIP 2 EMISSIVITY VALUES. THE PORTION OF SIMULATION MEASUREMENT ERROR ATTRIBUTED TO THE PSF USING c) CHIP 1 EMISSIVITY VALUES AND d) CHIP 2 EMISSIVITY VALUES. SCALES ARE IN RADIANCE °C DIFFERENCE.

Copyright © 2010 by ASME

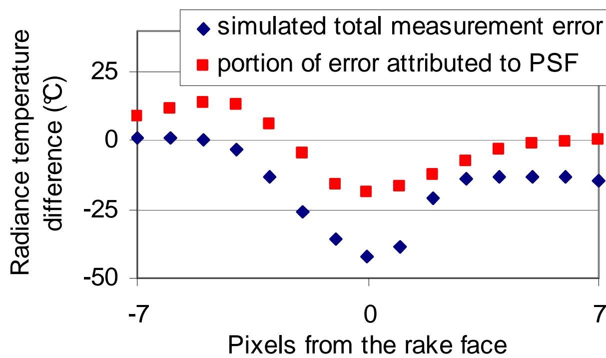

a)

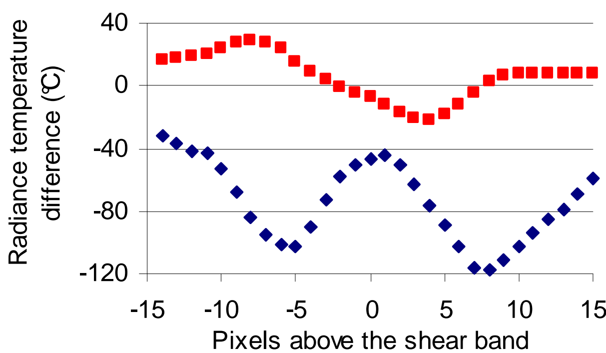

b)

FIGURE 11. MEASUREMENT ERROR DATA EXTRACTED FROM FIGURE 10. a) RAKE FACE MEASUREMENT ERROR USING CHIP 2 EMISSIVITY VALUES. b) SHEAR BAND MEASUREMENT ERROR USING CHIP 1 EMISSIVITY VALUES.

the difference in the standard deviation of the chip body emissivity values in Table 1 visibly affects the measurement error shown in Figure 10a and Figure 10b.

Closer analysis of the rake face measurement error in Figure 11a reveals that a measurement error of approximately -40 °C radiance temperature exists at the interface between the tool and the chip. Approximately half of this measurement error is attributable to the PSF. The large impact of the PSF is expected considering the difference in radiance temperature between the tool and the chip along the rake face resulting from the differences in emissivity, and considering the PSF acts as a filter, blending the radiance temperature of the tool and chip together.

Concerning the measurement error at the catastrophic shear band, greater measurement error occurs below and above the center of the shear band, where the measurement error approached -120 °C radiance temperature, whereas the center of the shear band only experienced a measurement error of -46 °C, with only -7 °C of that error attributable to the PSF. This results from the greater temperature gradient at the leading and trailing edges of the shear band. The PSF has less impact on the measurement error at the center of the shear band when compared to the rake face analysis. However, it should be noted that these results are dependent on the width of the shear band produced in the FEA. If the catastrophic shear band developed during the cutting experiments is narrower, the measurement error would be greater since the large temperature gradients would be closer together.

DISCUSSION

Comparison between simulation and experiment results encourage further development. Improving the simulation method will lead to verifying FEA results by directly comparing them with cutting process measurements. Also, the IR camera measurement error will be better understood, improving measurement uncertainty.

Shear band development must be better understood. The post-process chips used to determine emissivity only show fully developed catastrophic shear bands. Currently, the assumption is made that the mature shear band adequately represents the emissivity and width of the developing shear band. However, this may not be true (possibly due to relaxation of the chip after cutting) and could affect the data presented in Figure 9. Recent work at NIST using a single-spectrum high-speed (10^5 fps) visible camera has allowed several frames of the development of a shear band to be recorded, but this does not help in directly determining emissivity.

Reflections must be better understood to improve the understanding of measurement error. Most likely, reflections from the rake face to the nearby chip increase the apparent temperature of the chip along the rake face. This would occur because of the three-dimensional geometry of the side of the chip resulting from side-flow during formation and the higher emissivity of the tool. Reflections could explain why the lower emissivity values of chip 1 showed adequate comparison of the shear band with the experiment results, but underestimated the temperature near the rake face. It was expected that chip 1 would produce better emissivity values because the oxide layer appeared to affect the emissivity less than in chip 2 thus better representing the state of the chip when imaging the cutting process. The higher emissivity values of chip 2 produced a better match near the rake face because the increase in the emissivity due to the oxide layer helped to make up the difference resulting from not accounting for reflections. In addition, the effect of oxide layer on post-process chip emissivity must be better understood.

CONCLUSION

This paper presented the analysis method and results of simulating the IR camera measurement of segmented chip formation. The simulation used as input FEA results converted into radiance temperature using emissivity values obtained from post-process analysis of chips produced during experiments. The IR camera simulation accounted for integration time, size-of-source effect (both of which were the focus of an earlier investigation), and the PSF of the actual IR camera used in the experiments.

Copyright © 2010 by ASME

Comparison of the simulation results to experiment results showed good agreement. However, the best radiance temperature agreement of the chip area along the tool rake face occurred using the higher emissivity of the two post-process chips, while best agreement in the catastrophic shear band radiance temperature occurred using the lower emissivity of the two. Possible causes include reflections of the tool rake face along the edge of the chip, causing the measured temperature in the experiment to appear higher.

Measurement error analysis of the simulation results have shown that the PSF accounts for half of the >40 °C radiance temperature error at the tool-chip contact along the rake face. In contrast, the PSF accounts for less than 15 % of the 46 °C radiance temperature measurement error at a point in the center of the catastrophic shear band.

ACKNOWLEDGMENTS

The authors would like to thank Robert Ivester, Johannes Soons, Alkan Donmez, Shawn Moylan, and April Cooke of NIST for their support.

REFERENCES

[1] Heigel, J. C., Whitenton, E. P., (2009). "The Effects of Integration Time and Size-of-Source on the Temperature Measurement of Segmented Chip Formation Using Infrared Thermography." *Proceedings of the ASME International Manufacturing Science and Engineering Conference 2009*, October 4-7, West Lafayette, Indiana, USA, pp. 1-10.

[2] Kalpakjian, S., Schmid, S. R., (2003). "Manufacturing Processes for Engineering Materials." 4th Ed., *Pearson Education, Inc.*, Upper Saddle River, NJ.

[3] Johnson, G. R., Cook, W. H. (1983). "A Constitutive Model and Data for Metals Subjected to Large Strains, High Strain Rates and High Temperatures." *Seventh International Symposium on Ballistics,* April 19-21, The Netherlands, pp. 541-548.

[4] Marusich, T. D., Ortiz, M. (1995). "Modelling and Simulation of High-Speed Machining." *International Journal of Numerical Methods in Engineering,* 38(21), pp. 3675-3694.

[5] Jaspers, S. P. F. C., Dautzenberg, J. H. (2002). "Material behavior in conditions similar to metal cutting: flow stress in the primary shear zone." *Journal of Materials Processing Technology,* 122(2-3), pp. 322-330.

[6] Rhorer, R. L. (2003). "Dynamic Material Properties for Machining Simulation Using the NIST Pulse-Heated Kolsky Bar." *ASPE Proceedings*, October 26-31, Portland, Oregon, pp. 103-105.

[7] Davies, M. A., Ueda, T., M'Saoubi, R., Mullany, B., Cooke, A. L. (2007). "On the Measurement of Temperature in Material Removal Processes." *Annals of the CIRP*, 56(2), pp. 581-604.

[8] Whitenton, E., (2009). "Characterization of Uncertainties When Measuring Metal Cutting Temperatures Using Infrared Radiation Thermography." *Proceedings of SPIE*, 7299, pp. 1-12.

[9] Whitenton, E., Heigel, J., Ivester, R., (2008). "Measurement and Characterization of Dynamics in Machining Chip Segmentation." *Proceedings of the 11th CIRP Conference on Modeling of Machining Operations*, Gaithersburg, MD, pp.237-246.

[10] Heigel, J. C., Whitenton, E. P., (2009). "High-Speed Microvideography Observations of the Periodic Catastrophic Shear Event in Cutting AISI 1045 Steel." *Transactions of the North American Manufacturing Research Institution of SME*, 37, pp. 33-40.

[11] Ivester, R. W., Whitenton, E. P., Heigel, J. C., Marusich, T., Arthur, C., (2007). "Measuring Chip Segmentation by High-Speed Microvideography and Comparison to Finite-Element Modeling Simulations." *Proceedings of the 10th CIRP International Workshop on Modeling of Machining Operations*, Calabria, Italy, pp. 37-44.

[12] Ivester, R. W., Whitenton, E. P., (2003). "Simultaneous Visual and Infrared Imaging for Improved Machining Models." *NSF Workshop on Research Needs in Thermal Aspects of Material Removal Processes*, pp. 70-76.

[13] Heigel, J. C., Ivester, R. W., Whitenton, E. P., (2008). "Cutting Temperature Measurements of Segmented Chips Using Dual-Spectrum High-Speed Microvideography." *Transactions of the North American Manufacturing Research Institution of SME*, 36, pp. 73-80.

[14] Whitenton, E., Ivester, R., Yoon, H., (2005). "Simultaneous Visible and Thermal Imaging of Metals During Machining." *Proceedings of SPIE*, 5782, pp. 71-82.

[15] Whitenton, E., Cooke, A., Heigel, J., Aldamiz, I. A., (2010). "Recent Experiments Assessing the Uncertainty of Metal Cutting Temperature Measurements When Using the NIST High-Speed Dual-Spectrum Optical System." *Proceedings of SPIE, 7661, paper number 7661-18.*

[16] DeWitt, D. P., Nutter, G. D., (1988). "Theory and Practice of Radiation Thermometry." *John Wiley & Sons, Inc*, New York.

Copyright © 2010 by ASME